ACS APPLIED MATERIALS & INTERFACES

Research Article

www.acsami.org

Humidity Effects on Anisotropic Nanofriction Behaviors of Aligned Carbon Nanotube Carpets

J. Zhang, H. Lu, Y. Sun, L. Ci, P. M. Ajayan, and J. Lou*

Department of Mechanical Engineering and Materials Science, Rice University, Houston, Texas 77005, United States

Supporting Information

ABSTRACT: We evaluated the interfacial properties of vertically and transversely aligned multiwalled carbon nanotubes (CNTs) carpets using atomic force microscopy (AFM) under ambient (26%−52% relative humidity (RH)), mild (10% RH), and dry conditions (<3.3% RH). The frictional forces on a transversely aligned CNT (TAMWCNT) surface are lower than those on a vertically aligned CNT (VAMWCNT) surface, and they decrease as the relative humidity decreases for both TAMWCNT and VAMWCNT surfaces. Similar trends are found for adhesion forces on both surfaces. Contact mechanics theories are applied and compared in an attempt to better understand these results. The tribological behavior of CNT carpets unveiled in this paper is expected to inspire tunable friction surface engineering strategies.

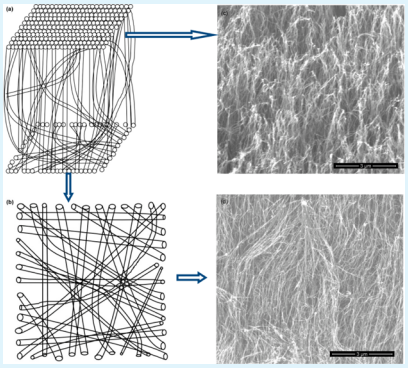

KEYWORDS: *carbon nanotube, humidity, anisotropy, adhesion and friction*

1. INTRODUCTION

As a ubiquitous phenomenon, friction occurs in virtually every aspect of life on a daily basis. The study of friction has consequently been carried out for more than five centuries. Carbon-based materials have been known to be excellent solid lubricants for many decades. Since their discovery by Iijima, multiwalled carbon nanotubes (MWCNTs)[1] and single-walled carbon nanotubes (SWCNTs)[2,3] continue to draw attention from the scientific community. Carbon nanotubes (CNTs) possess many unique properties, such as high tensile and flexural strength, high elastic modulus, and high aspect ratio;[4] these features, combined with the excellent tribological properties of carbon-based materials, have made CNTs attractive for use in applications at nanoscale levels, where friction is important, such as nanoelectromechanical systems (NEMS)[5] and nanocomposites.[6]

However, limited theoretical and experimental studies on CNTs friction properties have been reported, despite their exciting prospects in nanotribological applications. Ni et al.[7] simulated the friction between SWCNTs bundles and hydrogen-terminated diamond surfaces, and they concluded that the responses to the applied shear forces depend on the orientation. Specifically, bundles that were oriented vertically to the sliding surfaces had higher friction coefficients than transversally aligned bundles. Recently, the adhesion and friction behaviors of hierarchical vertically aligned CNT arrays were evaluated at multiple length scales using finite-element analysis (FEA) and molecular dynamics (MD) simulations.[8] It was unveiled that the adhesion force of laterally distributed CNT segments on top of vertically aligned CNT arrays could be enhanced by a factor of 5 and 10 at the macroscale and nanoscale levels, respectively. The tribological properties of CNT arrays were also examined in experiments. Kionshita et al.[9] showed extremely high friction coefficients of 1.0−2.2 for vertically aligned CNT forests 6 μm in length against gold tips of different radii. In addition, Dickrell et al.[10,11] found a very high friction coefficient (μ = 0.795) for vertically aligned CNT films grown on rigid substrates and a very low friction coefficient (μ = 0.090) for CNTs dispersed transversely on the same substrate. Moreover, they demonstrated the strong effects of surface chemistry and temperature on friction behaviors of both vertically and transversely oriented CNTs films. However, they reported that the frictional anisotropy was insensitive to humidity, which was a finding that needs to be further investigated, given the typical ambient environment for the intended application of such materials. The friction force in our system was found to be critically influenced by the relative humidity; with decreasing relative humidity, the friction force drops. One of the drawbacks for lateral force microscopy (LFM) is the small tip−sample contact area by using traditional atomic force microscopy (AFM) tips. Therefore, Lou and Kim[12] employed bare and aluminum-coated colloidal probes to quantify effects of interfaces on friction behavior of vertically aligned CNT arrays and found much higher friction forces for aluminum-coated colloidal probes, compared to bare borosilicate colloidal probes. Besides CNT arrays, the tribological properties of the individual nanotube were also examined using

Received: June 10, 2013
Accepted: September 4, 2013
Published: September 4, 2013

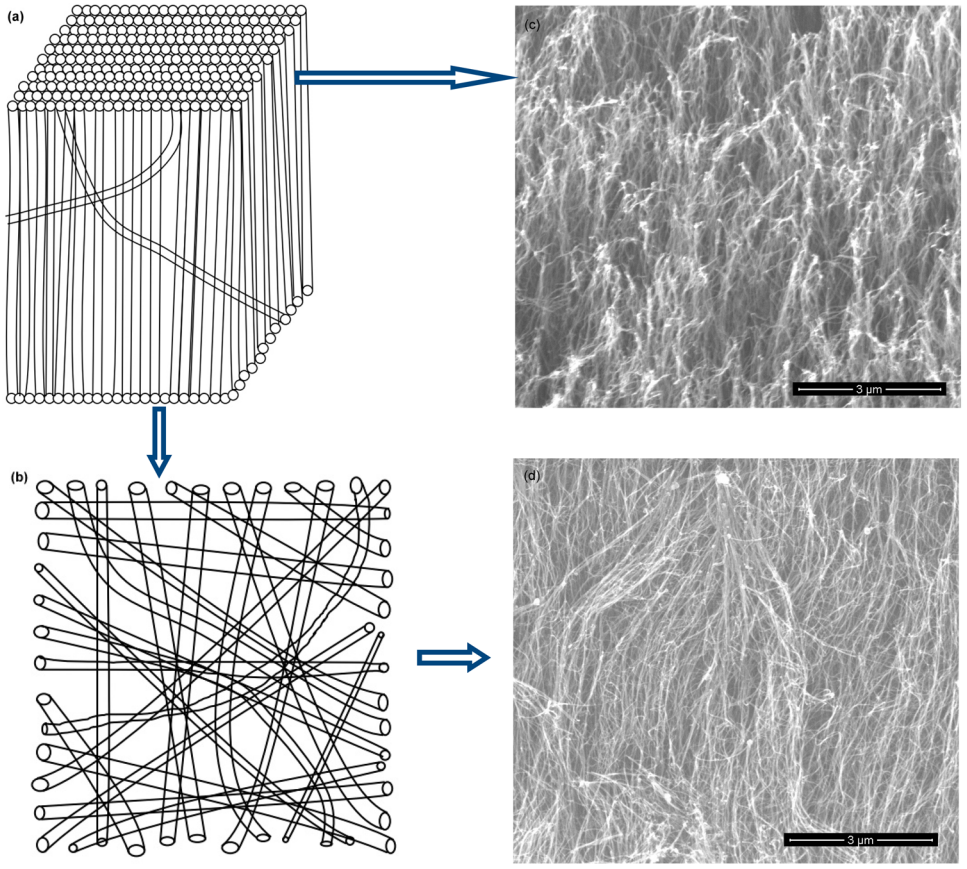

Figure 1. Schematic diagrams and scanning electron microscopy (SEM) images of vertically aligned carbon nanotubes (VAMWCNTs, top) and transversely aligned carbon nanotubes (TAMWCNTs, bottom): (a) schematic diagram showing a side view of the CNT carpet; (b) schematic diagram showing the TAMWCNTs (growth substrate removed for the sake of clarity); (c) SEM image showing a tilted (43°) view of the VAMWCNTs; and (d) SEM image showing a top view of TAMWCNTs.

MD simulation,[13] AFM,[14,15] and transmission electron microscopy (TEM) with a manipulator.[16]

In this study, we quantitatively evaluated the frictional properties of CNT carpets with two different tube orientations. The effects of relative humidity on friction and adhesion were thoroughly quantified in a chamber with a well-controlled environment for both vertically aligned and transversely aligned surfaces.

2. MATERIALS AND METHODS

Preparation of Carbon Nanotube Carpets. Multiwalled carbon nanotube (MWCNT) carpets with two different orientations were prepared using a xylene–ferrocene chemical vapor deposition (CVD) method. Typically, a xylene solution with a ferrocene concentration of 0.01 g/mL was used as carbon and catalyst precursors. During the CVD process, an Ar/H_2 gas mixture (15 vol % H_2) was flowed through the reactor tube at a rate of 300 sccm. The xylene solution was fed to a preheating zone of 180 °C by a flux pump continuously at a feeding rate of 0.11 mL/min; that solution then became a vapor and was carried by Ar/H_2 gas (100 sccm) into the 770 °C growth zone. CNT blocks several millimeters thick could be prepared easily within a few hours (1–4 h). Because of the nature of this growth process, the bottom side of the MWCNT carpets has a much better vertical alignment, compared to the top side, where MWCNTs tend to align more in the transverse direction, which is parallel to the growth substrate, given the two MWCNT orientations studied here. After sample transfer, the transversely aligned side was flipped downward. In order to illustrate the relative orientation and surface morphology of CNTs carpet, schematic diagrams of the CNT carpet and the corresponding aligned CNT surface are shown in Figure 1. The morphology and individual diameter of CNTs arrays were characterized by scanning electron microscopy (SEM) and TEM. Raman spectra were recorded using a Raman microscopy system that was equipped with a 514.5-nm excitation source, to confirm that the carbon nanotubes in the transversely aligned surface retained their character after regrowth. Static contact angles were measured by placing droplets of deionized (DI) water on the surface of CNTs layers.

Colloidal Probe Preparation. A stable AFM signal could not be obtained using a sharp AFM tip, because the supersharp tip penetrated deeply into the soft CNT arrays. Thus, a colloidal probe with a tip radius of 10 μm was employed to quantify the friction behavior of this CNT carpet. Borosilicate glass microspheres (10.0 ± 1.0 μm in diameter; Duke Scientific Corporation) were attached, with the aid of a micromanipulator (Model No. 6200), to regular AFM cantilevers, using Devcon 5-minute Epoxy adhesive.

Experimental Procedures. Lateral force microscopy (LFM) (Pico plus, Agilent) evaluations were executed on both the VAMWCNT side and the TAMWCNT side. LFM scans were performed by progressively decreasing the normal load approximately every 16 scans or so, to measure the frictional force as a function of the applied normal load. Both the VAMWCNT and TAMWCNT sides were scanned at three

different locations to ensure the proper representation of the sample surfaces. Scans were also repeated over the exact same location to check the reproducibility of the experiment. The test was run with a scan size of 10 μm at a scan speed of 12 μm/s.

To quantify the adhesion forces between the nanotube surfaces and the AFM probe, force versus distance spectroscopy was run on both sides and the amount of adhesion was calculated. The adhesion forces were repeated three times at each location and at three different locations on each side. Humidity of the testing environment was controlled using an environmental isolation chamber. A controlled flow of nitrogen gas was used to create a dry environment with relative humidity (RH) values of <5% (dry conditions) and ~10% (mild conditions). Both relative humidity and temperature were monitored using a digital hygrometer/thermometer before, during, and after the actual testing. The testing conditions are summarized in Table S1 in the Supporting Information.

3. RESULTS AND DISCUSSION

SEM images of the transversely and vertically aligned CNTs arrays are shown in Figure 1. The TAMWCNT side comprises a distributed ensemble of entangled nanotubes oriented randomly in the horizontal plane. The vertically aligned side has the last few micrometers of the top surface entangled and intertwined. The diameter of the individual nanotube is ~10 nm, as shown in Figure S1 in the Supporting Information. Because of the high anisotropy of the sample geometry, along with anisotropy in mechanical, electrical, and thermal properties of individual CNTs,[17−21] it is expected that the frictional behavior of nanotubes is highly orientation-dependent. The Raman spectra of both surfaces are displayed in Figure 2, the

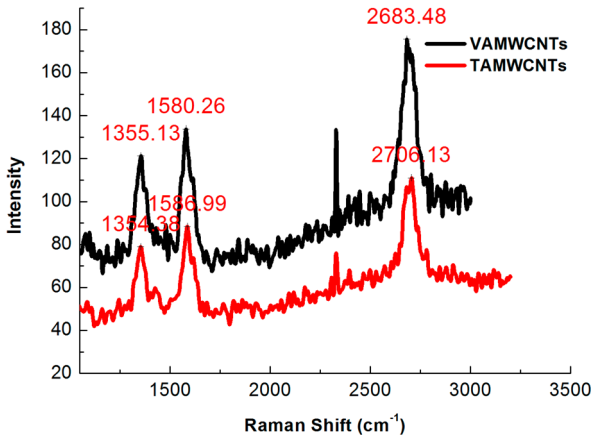

Figure 2. Raman spectra of both surfaces; the shifts in CNT characteristic Raman peaks that are attributable to the compression strain do not affect the tribological behavior of CNT arrays.

spectra of which have pronounced features at 1355 cm^{-1} (D-mode), ~1580 cm^{-1} (G-mode), and ~2683 cm^{-1} (2D-mode) for VAMWCNTs, and at 1354 cm^{-1} (D-mode), ~1586 cm^{-1} (G-mode), and ~2706 cm^{-1} (2D-mode) for TAMWCNTs. The intensity ratio of the D-band to the G-band is 0.89 for both spectra. The shift in the disorder-induced second-order Raman peak is due to the residue compression strain,[22,23] which does not influence the tribological properties of MWCNTs.

The variation of frictional force with applied normal load for the TAMWCNT array in the ambient environment (47.2%−51.3% RH) and for the VAMWCNT array under ambient conditions (26.1%−41.3% RH) are displayed in Figure 3a. Data from multiple tests overlap closer on the transversely aligned surface, compared to the vertically aligned surface. This data overlap on the transversal surface reflects the more-homogeneous local surface characteristics. Clearly, the frictional force is higher on a vertically aligned CNT surface than on a horizontally aligned CNT surface, as predicted by MD simulations.[7] The frictional coefficient values of each test are calculated and shown in Figure 3b. In air, the frictional coefficient values are obviously larger for VAMWCNTs than those of TAMWCNTs. The average value is μ = 0.545 with a standard deviation of σ = 0.057 for the vertically oriented side, and the average value is μ = 0.167 with a standard deviation of σ = 0.015 for the transversely aligned side.

To investigate the possible relationship between humidity and frictional properties, scans were also done at the other two different humidity levels, as described earlier. Frictional forces of VAMWCNTs and TAMWCNTs plotted against normal load under both conditions are shown in Figures 4a and 5a. The variation of humidity is found to have a strong effect on frictional force. Figure 4a shows that, under dry conditions, friction is again higher on the VAMWCNT side than on the TAMWCNT side. Similarly, Figure 5a shows that, when the relative humidity is ~10%, the frictional force on the VAMWCNT surface dominates over that observed on the TAMWCNT surface. Although some researchers have demonstrated that humidity had an insignificant effect on the vertically aligned CNTs, because of their highly hydrophobic characteristics,[24−26] our observations were different: The friction forces are apparently dependent upon the RH levels, according to results shown in Figures 3−5, regardless of the orientation of the sample. Figures 4b and 5b show the coefficient of friction values of each orientation under both dry and mild conditions. Under dry conditions, μ = 0.184 with σ = 0.013 for the vertically aligned side and μ = 0.091 with σ = 0.018 for the transversely aligned side. Similarly, under mild conditions, μ = 0.342 with σ = 0.029 for the vertically aligned surface and μ = 0.173 with σ = 0.025 for the transversely aligned surface.

To better demonstrate the effects of relative humidity on the resultant frictional forces on both surfaces, the average frictional forces calculated from Figures 3−5 are plotted against the applied normal load at all three humidity levels in Figure 6, for the sake of clarity. In all cases, the humidity dependence on the frictional forces is present, but with characteristic differences depending on the CNTs orientations. For vertically aligned CNTs, the average frictional forces increase significantly as the relative humidity increases; for transversely aligned CNTs, the difference in average frictional forces is not evident when the relative humidity is increased to the mild level (~10% RH). The slight difference on transversal surface may be ascribed to the surface geometry of the TAMWCNTs, which attains water molecule saturation more easily.

Discussions. The variation of frictional force in different orientations is probably due to the fact that nanotubes are flexible in the direction perpendicular to the axis direction and stiff in the direction parallel to the axis. The vertically aligned CNTs could buckle or bend in response to compression, and they could lean in the direction of sliding, which would cause more energy dissipation and, therefore, higher friction.[7] Interestingly, our experiments showed a clear dependence of friction on the relative humidity. A humidity increase can

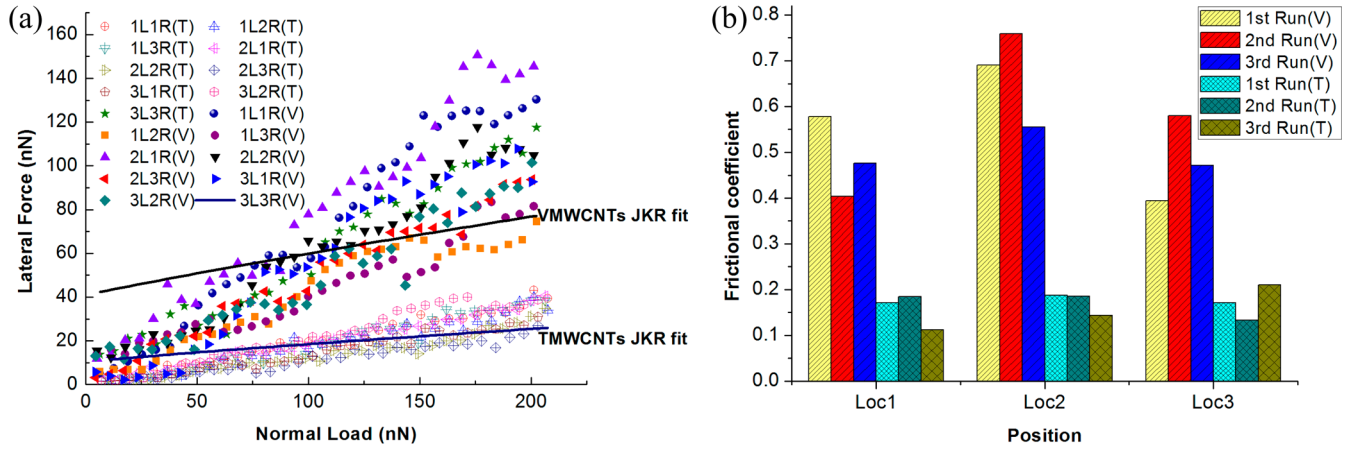

Figure 3. (a) Frictional force versus applied normal load under ambient conditions for TAMWCNTs and VAMWCNTs. Solid lines represent the Johnson−Kendall−Roberts (JKR) fit. Legends marked with "T" denote TAMWCNTs whereas those marked with "V" denote VAMWCNTs. (b) Friction coefficients summary. The frictional forces (frictional coefficients) on the vertically aligned CNT surface are much higher than those on the transversely aligned CNT surface under ambient conditions (26%−52% RH).

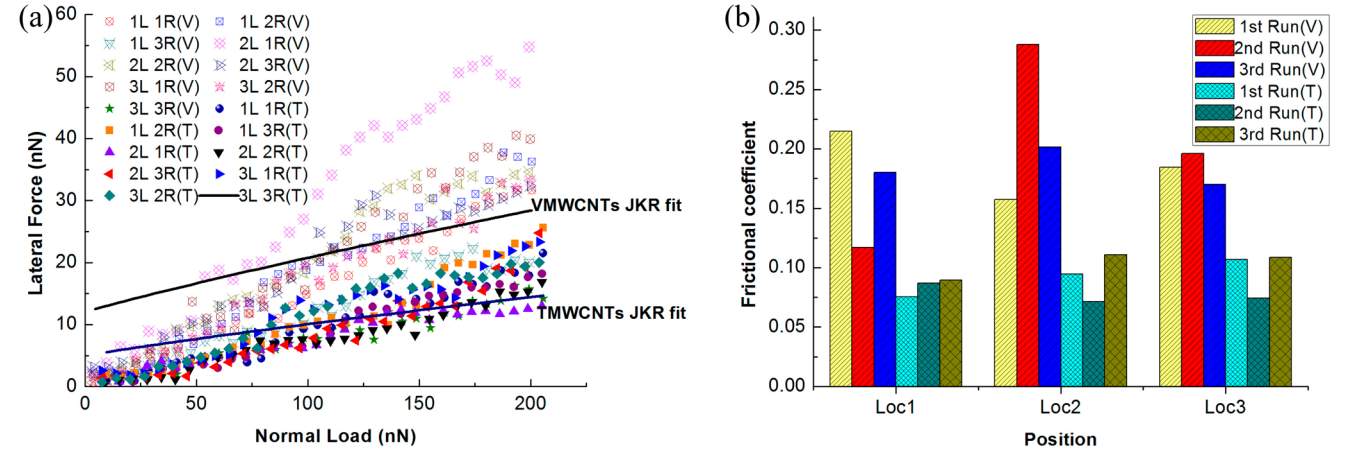

Figure 4. (a) Frictional force versus applied normal load under dry conditions for TAMWCNTs and VAMWCNTs. Solid lines show the JKR fit. (b) Friction coefficients summary. The frictional forces (frictional coefficients) on the vertically aligned CNT surface are slightly higher than those on the transversely aligned CNT surface under dry conditions (<3.3% RH).

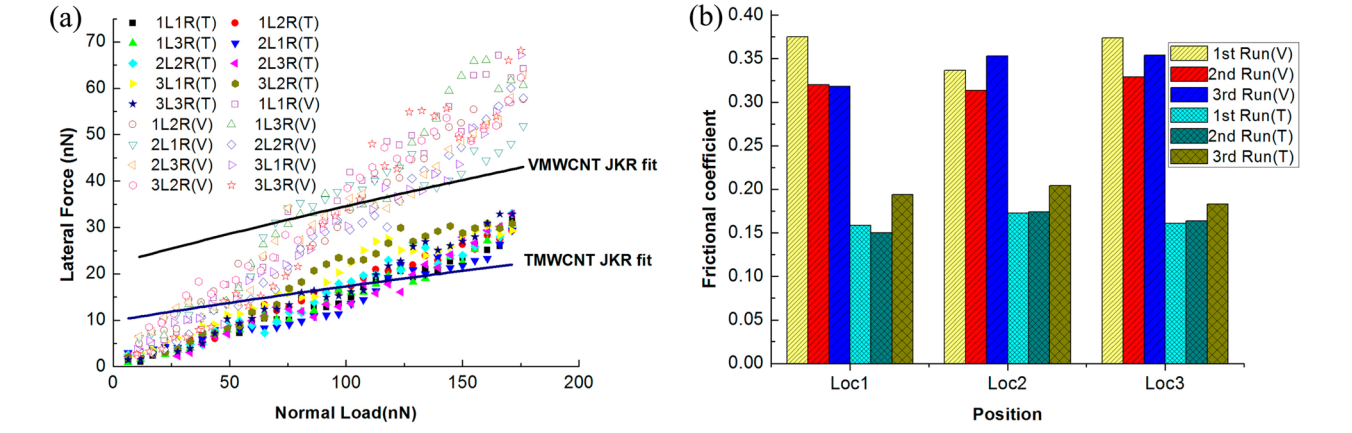

Figure 5. (a) Frictional force versus applied normal load under mild conditions for TAMWCNTs and VAMWCNTs. Solid lines show the JKR fit. (b) Friction coefficients summary. The frictional forces (frictional coefficients) on the vertically aligned CNT surface are higher than those on the transversely aligned CNT surface under dry conditions (~10% RH).

provoke the formation of small area water pucks near contact regions, which could cause capillary interaction with the AFM tip affecting friction properties.[27] Therefore, the presence of even a very small amount of water molecules could have a significant effect on friction properties of a seemly hydrophobic surface. We independently measured and compared the static contact angles of water droplets on both CNT surfaces. Images of water droplets sitting on these surfaces are shown in Figure

dx.doi.org/10.1021/am402221u | ACS Appl. Mater. Interfaces 2013, 5, 9501−9507

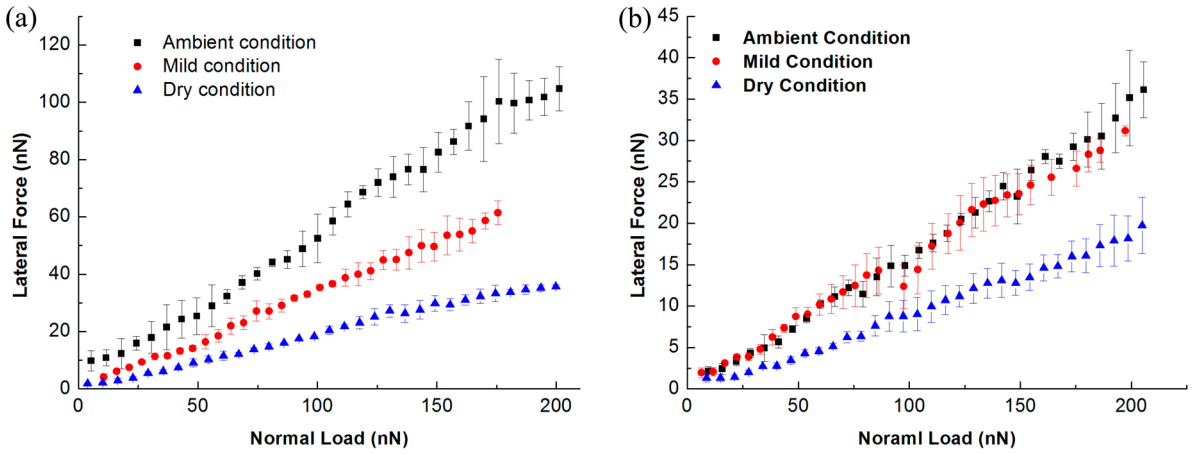

Figure 6. Average frictional force versus applied load, as a function of humidity, for (a) VAMWCNTs and (b) TAMWCNTs. The frictional forces on the vertically aligned surface are more sensitive, with regard to relative humidity, than those on the transversely aligned surface.

S2 in the Supporting Information. The contact angle of water on VAMWCNTs array was measured to be 131° (see Figure S2(a) in the Supporting Information), whereas that on the TAMWCNTs array was 145° (see Figure S2(b) in the Supporting Information). This difference in contact angle indicates the possible differences of water molecule adsorption capability in the two orientations, by which it could shed some light onto the observed differences in frictional properties.

Next, we employed contact mechanics theories, which will be briefly described below for a more quantitative understanding of our results. The relationship that the "lateral" frictional force (F_L) is proportional to the real contact area (A), and to a mean lateral force per unit area, via the shear strength (τ), was proposed by Bowden and Tabor in 1950.[28]

$$F_L = \tau A \tag{1}$$

Meanwhile, realizing the importance of interfacial adhesive forces on friction behaviors, Derjaguin proposed the following modified version of Amonton's equation for adhering surfaces:

$$F = \mu(L_c + L) = F_c + \mu L \tag{2}$$

where a constant "internal" load L_c is added to the external load L to account for the absolute value of intermolecular adhesive forces.[29] From this relationship, it is reasonable to expect that the humidity could affect the adhesion forces as it would affect frictional forces for the similar interface under similar testing conditions, if neglecting the factors of the surface nanoroughness or microroughness, as well as the different deformation modes. Furthermore, if the elastic deformation caused by adhesive forces is large compared to their range of action, the contact area (as well as the critical pull-off forces) can be expressed in terms of Johnson–Kendall–Roberts (JKR) theory[12,30] in the following way:

$$A = \pi\left\{\frac{R}{K}\left[L - 2L_c + \sqrt{4L_c(L_c - L)}\right]\right\}^{2/3} \tag{3a}$$

with

$$L_c(\mathrm{JKR}) = -\frac{3}{2}\pi R\omega_a \tag{3b}$$

Here, R is the tip radius, ω is the work of adhesion (interface energy), and K is the contact modulus, which is defined as

$$K = \frac{4}{3}\left(\frac{1-\nu_{tip}^{\ 2}}{E_{tip}} + \frac{1-\nu_{sample}^{\ 2}}{E_{sample}}\right)^{-1} \tag{4}$$

In contrast, if the elastic deformation is small, compared to the range of adhesive forces, the contact area and the critical pull-off forces can employ Derjaguin–Muller–Toporov (DMT) theory[12,30] to describe

$$A = \pi\left[\frac{R}{K}(L + L_c)\right]^{2/3} \tag{5a}$$

with

$$L_c(\mathrm{DMT}) = -2\pi R\omega_a \tag{5b}$$

If the shear strength τ is assumed to be constant, then the above solutions for contact area can be directly fitted to the friction data obtained earlier in Figures 3–5. We let the radius of the AFM tip and the contact modulus be free parameters. Both the JKR and DMT theories were used to fit the result gained from VAMWCNT and TAMWCNT surfaces. Generally, both the JKR and DMT theories work for transversely aligned nanotubes under different conditions (DMT fitting curve not shown). However, neither theory fit particularly well with the results for VAMWCNTs at different humidity levels.

Given the critical importance of adhesive forces for nanoscale friction behaviors,[30] adhesion measurements were made for both surfaces under similar humidity conditions. The adhesive forces of VAMWCNTs and TAMWCNTs in different environments are summarized in Table 1. The average adhesive forces of TAMWCNTs are apparently lower than those of VAMWCNTs. With regard to the adhesion data of TAMWCNTs, no significant distinctions were observed, especially for higher humidity levels, similar to the trend observed in Figure 6b. Whereas, for VAMWCNTs, the effect of humidity on adhesion is very clear, with the adhesive forces decreasing as RH decreases. The observed adhesion difference is in agreement with the previous assumption that friction would be greater due to the stronger adhesive force induced by the surface water layer formed under ambient conditions. Another interesting phenomenon is that the standard deviations of the adhesive force on both sides were high, which might relate to the surface roughness of MWCNTs.

dx.doi.org/10.1021/am402221u | ACS Appl. Mater. Interfaces 2013, 5, 9501–9507

Table 1. Adhesive Force for VAMWCNTs and TAMWCNTs under Different Relative Humidity Levels

sample and testing conditions	average adhesion (nN)	standard deviation (nN)
VAMWCNTs		
dry conditions[a]	61.33	10.51
mild conditions[b]	79.75	9.56
ambient conditions[c]	99.32	16.75
TAMWCNTs		
dry conditions[a]	42.12	7.29
mild conditions[b]	57.35	8.80
ambient conditions[c]	57.84	13.59

[a]Relative humidity of <5%. [b]Relative humidity of ~10%. [c]Relative humidity of 26%−52%.

In order to estimate the critical pull-off (adhesive) forces from contact mechanics theories, the surface energies for both VA-MWCNT and TA-MWCNT surfaces must be determined. Here, we first assume that the total, dispersive, and polar components of the liquid surface free energy (γ_l, γ_l^d, and γ_l^p, respectively) are known and then measure the corresponding contact angles of the liquids used, as shown in Table S2 in the Supporting Information. Two plots according to eq S1, given in the Supporting Information, using the contact angles of three testing liquids measured in this study, are shown in Figure S3 in the Supporting Information. We estimated the polar (γ_l^p) and dispersive (γ_l^d) components of the surface free energy of each carpet surface from the slope and the intercept of the linear fit in Figure S4 in the Supporting Information. The total surface free energy, $\gamma_s^p + \gamma_s^d$, for TA-MWCNTs was calculated to be 0.74 mJ/m^2, and that for VAMWCNT was determined to be 2.16 mJ/m^2. By applying the surface energy of silicon oxide for glass ($\gamma_{SiO_2} \approx 115$ mJ/m^2), the work of adhesion for the glass/TAMWCNT interface can be estimated by the relation $\omega_a = 2(\gamma_{TA\text{-}MWCNT}\gamma_{SiO_2})^{1/2} \approx 18.5$ mJ/m^2, whereas the work of adhesion for the glass/VAMWCNT interface is described by the relation $\omega_a = 2(\gamma_{VA\text{-}MWCNT}\gamma_{SiO_2})^{1/2} \approx 31.5$ mJ/m^2. Both eq 3b and eq 5b were employed to calculate the critical pulling forces. One thing that should be mentioned is that the local contact radius of curvature is smaller than the radius of curvature of the attached bead (see Figure S5 in the Supporting Information). The representative radius of curvature of 1000 nm is applied here, which gives critical pulling forces of 87 nN (JKR theory) and 116 nN (DMT theory) for TAMWCNTs, and 148 nN (JKR theory) and 198 nN (DMT theory) for VAMWCNTs. According to those estimations, the JKR theory estimation seems to be more consistent with the experimental value (see Table 1), which indicates that the JKR theory might be a better option for both VAMWCNTs and TAMWCNTs.

4. CONCLUSIONS

In summary, the friction and adhesion properties of vertically and transversely aligned carbon nanotube (CNT) carpets were evaluated under different relative humidity levels. The vertically aligned multiwalled carbon nanotube (VAMWCNT) surface consistently generates higher friction at all humidity levels, compared to the transversely aligned multiwalled carbon nanotube (TAMWCNT) surface. Frictional forces are found to be higher in ambient environment than under the dry or mild humidity conditions for both surfaces, while a similar dependence on relative humidity and nanotube orientation is found for adhesion forces. The variations in friction coefficients are shown to be also dependent on the nanotube orientation in carpet as well as the humidity level. This research provides the possibility to rationally engineer surface domains to be either low friction or high friction through control of nanotube orientations, when effects of humidity are carefully taken into consideration.

■ ASSOCIATED CONTENT

Supporting Information

The static contact angle measurement and AFM probe surface topography. This material is available free of charge via the Internet at http://pubs.acs.org/.

■ AUTHOR INFORMATION

Corresponding Author

*E-mail: jlou@rice.edu.

Notes

The authors declare no competing financial interest.

■ ACKNOWLEDGMENTS

The authors gratefully thank the support from the Welch Foundation (through Grant No. C-1716), AFOSR MURI (FA9550-12-1-0035), and the AFOSR Grant No. FA9550-13-1-0084.

■ REFERENCES

(1) Iijima, S. *Nature* **1991**, *354*, 56−58.
(2) Iijima, S.; Ichihashi, T. *Nature* **1993**, *363*, 603−605.
(3) Bethune, D. S.; Kiang, C. H.; de Vries, M. S.; Gorman, G.; Savoy, R.; Vazquez, J.; Beyers, R. *Nature* **1993**, *363*, 605−607.
(4) Sinnott, S. B.; Andrews, R. *Crit. Rev. Solid State Mater. Sci.* **2001**, *26*, 145−249.
(5) Sinnott, S. B.; Aluru, N. *Carbon Nanotechnology: Recent Developments in Chemistry, Physics, Materials Science and Device Applications*, 1st Edition; Dai, L. M., Ed.; Elsevier: Amsterdam, 2006; p 361.
(6) Ajayan, P. M.; Schadler, L. S.; Giannaris, C.; Rubio, A. *Adv. Mater.* **2000**, *12*, 750−753.
(7) Ni, B.; Sinnott, S. B. *Surf. Sci.* **2007**, *487*, 87−96.
(8) Hu, S.; Xia, Z.; Gao, X. *ACS Appl. Mater. Interfaces* **2012**, *4*, 1972−1980.
(9) Kinoshita, H.; Kume, I.; Tagawa, M.; Ohmae, N. *Appl. Phys. Lett.* **2004**, *85*, 2780−2781.
(10) Dickrell, P. L.; Sinnott, S. B.; Hahn, D. W.; Raravikar, N. R.; Schadler, L. S.; Ajayan, P. M.; Sawyer, W. G. *Tribol. Lett.* **2005**, *18*, 59−62.
(11) Dickrell, P. L.; Pal, S. K.; Bourne, G. R.; Muratore, C.; Voevodin, A. A.; Ajayan, P. M.; Schadler, L. S.; Sawyer, W. G. *Tribol. Lett.* **2006**, *24*, 85−90.
(12) Lou, J.; Kim, K. S. *Mater. Sci. Eng., A* **2008**, *483*, 664−667.
(13) Schall, J. D.; Brenner, D. W. *Mol. Simul.* **2000**, *25*, 73−78.
(14) Falvo, M. R.; Steele, J.; Taylor, R. M.; Superfine, R. *Phys. Rev. B* **2000**, *62*, 10664−100667.
(15) Falvo, M. R.; Taylor, R. M.; Helser, A.; Chi, V.; Brooks, F. P.; Washburn, S.; Superfine, R. *Nature* **1999**, *397*, 236−238.
(16) Suekane, O.; Nagataki, A.; Mori, H.; Nakayama, Y. *Appl. Phys. Express* **2008**, *1*, No. 064001.
(17) Langer, L.; Stockman, L.; Heremans, J. P.; Bayot, V.; Olk, C. H.; Van Haesendonck, C.; Bruynseraede, Y.; Issi, J. P. *J. Mater. Res.* **1994**, *9*, 927−933.
(18) Heremans, J.; Olk, C.; Morelli, D. *Phys. Rev. B* **1994**, *49*, 15122−15125.
(19) Langer, L.; Bayot, V.; Grivei, E.; Issi, J. P.; Heremans, J. P.; Olk, C. H.; Stockman, L.; Van Haesendonck, C.; Bruynseraede, Y. *Phys. Rev. Lett.* **1996**, *76*, 479−482.

(20) ISSI, J. P.; Langer, L.; Heremans, J.; Olk, C. H. *Carbon* **1995**, *33*, 23−27.
(21) Treacy, M. M. J.; Ebbesen, T. W.; Gibson, J. M. *Nature* **1996**, *381*, 678−680.
(22) Schadler, L. S.; Giannaris, S. C.; Ajayan, P. M. *Appl. Phys. Lett.* **1998**, *73*, 3842−3844.
(23) Ganesan, Y.; Lou, J. *J. MEMS* **2009**, *61*, 32−37.
(24) Ler, J. G. Q.; Hao, Y. F.; Thong, J. T. L. *Carbon* **2007**, *45*, 2737−2743.
(25) Ohmae, N. *Tribol. Int.* **2006**, *39*, 1497−1502.
(26) Turq, V.; Ohmae, N.; Martin, J. M.; Fontaine, J.; Kinoshita, H.; Loubet, J. L. *Tribol. Lett.* **2005**, *19*, 23−28.
(27) Weisenhorn, A. L.; Maivald, P.; Butt, H. J.; Hansma, P. K. *Phys. Rev. B* **1992**, *45*, 223−226.
(28) Bowden, F. P.; Tabor, D. *The Friction and Lubrication of Solids*; Oxford University Press: Oxford, U.K., 1950; p 67.
(29) Derjaguin, B. V. *Z. Phys.* **1934**, *88*, 661−675.
(30) Carpick, R. W.; Salmeron, M. *Chem. Rev.* **1997**, *97*, 1163−1194.